Monolayer doping of silicon-germanium alloys: a balancing act between phosphorus incorporation and strain relaxation.

Noel Kennedy,[1,2,3] Ray Duffy,[*2] Gioele Mirabelli,[2] Luke Eaton,[1,2,3] Nikolay Petkov,[4] Justin D. Holmes,[1,2,3] Chris Hatem,[5] Lee Walsh,[2] and Brenda Long*[1,2,3]

[1]School of Chemistry, University College Cork, Cork, T12 YF78, Ireland.

[2]Tyndall National Institute, Lee Maltings, Cork, T12 R5CP, Ireland.

[3]CRANN@AMBER, Trinity College Dublin, Dublin 2, D02 E16, Ireland.

[4]Cork Institute of Technology, Bishopstown, Cork, T12 T66T, Ireland.

[5]Applied Materials, Gloucester, Massachusetts, MA 01930, USA

Address correspondence to: brenda.long@ucc.ie, ray.duffy@tyndall.ie

KEYWORDS: Monolayer doping; silicon-germanium; strain relaxation.

ABSTRACT

This paper presents the application of monolayer doping (MLD) to silicon-germanium (SiGe). This study was carried out for phosphorus dopants on wafers of epitaxially grown thin films of strained SiGe on silicon with varying concentrations of Ge (18, 30 and 60 %). The challenge presented here is achieving dopant incorporation while minimising strain relaxation. The impact of high temperature annealing on the formation of defects due to strain relaxation of these layers was qualitatively monitored by cross-section transmission electron microscopy (XTEM) and atomic force microscopy (AFM) prior to choosing an anneal temperature for the MLD drive-in. Though the bulk SiGe wafers provided are stated to have 18, 30 and 60 % Ge in the epitaxial SiGe layers it does not necessarily mean that the surface stoichiometry is the same and this may impact the reaction conditions. X-ray photoelectron spectroscopy (XPS) and angle-resolved XPS were carried out to compare the bulk and surface stoichiometry of SiGe to allow tailoring of the reaction conditions for chemical functionalization. Finally, dopant profiling was carried out by secondary ion mass spectrometry (SIMS) to determine the impurity concentrations achieved by MLD. It is evident from the results that phosphorus incorporation decreases for increasing mole fraction of Ge, when the rapid thermal annealing temperature is a fixed amount below the melting temperature of each alloy.

INTRODUCTION

Device sizes for electronic applications have been aggressively scaled down over the past 50 years, pushing the limits of what was capable by introducing new materials such as high-k dielectrics,[1] and new device architectures such as FinFETs,[2] for example. Regardless, in recent times device dimensions have approached a critical point where silicon, the cornerstone of the semiconductor industry, struggles to achieve the performance gains as scaling continues. In this context, other high mobility materials, such as SiGe, are being investigated to assess their potential.[3] Currently, low mole fraction (MF) SiGe is being used as a stress enhanced carrier mobility booster[4] and is considered to be a viable candidate for a channel material in MOSFETs.[5-7] Recently, the 7-nm technology node solution has also been proposed with integration of SiGe p- and strained-Si n-MOSFETs, showing the feasibility of SiGe devices in future devices.[8] However, there are no reports of chemical functionalization of SiGe in literature, and only a few reports of *ex-situ* doping SiGe[9, 10] when compared to silicon. For thin-film homogeneous strained or relaxed SiGe with >50 % Ge-content there is little available experimental data on processing such as dopant diffusion and activation, contact formation, or on *in-situ* doping and selective epitaxial growth on surfaces with different crystal orientations. Very recently, publications have emerged on high-Ge content SiGe for solar cell applications.[11-13]

Doping of future technology devices fabricated either from thin-films or 3-dimensional structures could prove difficult for ion implantation, which has been the most commonly used *ex-situ* doping technique during the device miniaturization drive until this point.[14, 15] High energy ion beams induce damage (amorphization) into these structures which prove difficult to remove, if at all.[16] Possibly the most critical flaw of ion implantation is the lack of conformality seen when doping 3-dimensional structures such as fins or nanowires. Due to the directionality of the technique it struggles to equally dope both the top and sidewalls of these

structures.[17] A number of alternative *ex-situ* doping methods have been proposed and developed to offer solutions to the problems encountered with ion implantation such as plasma doping (PLAD),[18] spin-on-doping,[19] and solid-source-diffusion.[20] However, these techniques also suffer from crystal damage or lack of dose control. Doping SiGe *in-situ* has been studied for many years[21-23] and is the current trend in certain technology applications. Furthermore a boost in dopant activation by using a laser anneal after the growth of the *in-situ* doped epi layer has shown to be beneficial in source/drain contact regions.[24] However for alternative applications, or other parts of the transistor, epitaxy may not be suitable due to design or space restrictions.

Monolayer doping (MLD) has been developed as a method to produce ultra-shallow junctions (USJ's) without crystal damage, while also conformally doping 3-dimensional substrates.[25-27] It has already been demonstrated on a variety of semiconductors including Si,[28-34] Ge,[35-37] and a number of III-V materials.[38] **Figure 1** depicts the MLD procedure on SiGe. The key step involves functionalization of the target surface through the bonding of a dopant molecule (in this case allyldiphenylphosphine (ADP)) to form a self-limiting monolayer where the quantity of dopant molecules present is determined by the molecule size and also defines the dose. Once monolayer formation is complete the samples are capped with an oxide layer to prevent desorption and promote diffusion of the dopant atoms into the substrate during thermal treatments. After thermally treating the samples the capping layer can be removed to leave a uniformly doped substrate whether it be planar or 3-dimensional. This paper will examine the application of phosphorous MLD to SiGe alloys ranging from low Ge content 18 %, to high Ge content 60 % aiming to understand if this novel doping technique can effectively dope these substrates. There are two main challenges associated with doping SiGe by MLD 1) How to chemically functionalize the SiGe with dopant-containing molecules (i.e. will the reactivity of

the surface atoms to the molecules be like silicon or germanium?) and 2) How to avoid strain relaxation of the non-buffered SiGe layers during the dopant drive-in annealing step?

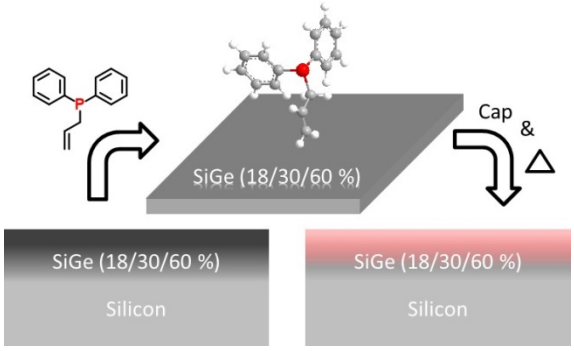

Figure 1: Summary of MLD procedure on SiGe

EXPERIMENTAL

Thin films of strained SiGe were grown on a 300 mm Applied Materials epitaxy system on silicon substrates with germanium contents of 18, 30 and 60 % respectively. The thickness of these films was inspected with cross sectional transmission electron microscopy (X-TEM). All chemicals were purchased from Sigma Aldrich. 1×1 cm samples were cut from the starting SiGe wafers and cleaned by sonicating in acetone (≥99.8 %) for 2 minutes, followed by a rinse in isopropyl alcohol (IPA-99.9 %) and drying under a stream of nitrogen. Samples were hydrogen terminated by dipping in 2 % hydrofluoric acid (HF) for 10 seconds and placed under nitrogen in a Schlenk line to prevent re-oxidation. A 0.1 M solution of allyldiphenylphosphine (ADP-95 %) in mesitylene (98 %) was degassed and transferred into the reaction flask containing the H-terminated samples. This reaction flask was heated to 180 °C for 3 hours to allow for optimal monolayer formation on the SiGe surface. Samples were then removed and sonicated in IPA for 1 minute followed by a further IPA rinse and drying under a stream of nitrogen to remove any physisorbed dopant molecule. Functionalized samples were stored under nitrogen until capping with 50 nm sputtered SiO_2. Rapid thermal annealing (RTA) was

carried out at a variety of temperatures and times which are specified for each result. The SiO_2 capping layer was then removed by dipping in a 25:1 BOE solution until a hydrophobic H-terminated surface was produced.

SIMS data was acquired on a Phi Adept 1010 using a 0.5-1 keV Cs+ bombardment with negative ion detection. Calibration was carried out using SiGe which has been implanted with P and measured using RBS (Rutherford backscattering spectrometry) to determine composition. AFM was implemented in tapping/noncontact mode at room temperature over a 3×3 μm scanning area. A Kratos ULTRA spectrometer was used for XPS measurements with the following parameters. Sample temperature was kept between 20-30 °C with a monochromated Al K α source used. Pass energies of 160 eV for survey spectra and 20 eV for narrow regions were used with steps of 1 eV (survey) and 0.05 eV (narrow regions). Dwell times were 50 ms (survey) and 100 ms (regions) while 12 sweeps were carried out during survey spectra and for narrow region analysis from 5-40 sweeps were used. For structural analysis, FEI's Dual Beam Helios Nanolab 600i system using Ga ion beam was used to obtain cross-section samples. Electron beam C, electron beam Pt, and ion beam C were used as protective layers. Lamellas were thinned and polished at 30 kV 100 pA and 5 kV 47 pA, respectively. JEOL 2100 HRTEM operated at 200 kV in Bright Field mode using a Gatan Double Tilt holder was used for XTEM imaging.

RESULTS AND DISCUSSION

Figure 1 broadly describes the process of doping SiGe by MLD. ADP was chosen as a source of phosphorus for these experiments for two reasons. (1) It contains the C=C functionality which reacts with both Ge and Si, an assumption being made that it will also react with SiGe and (2) its remaining functional groups are phenyl rings which are highly unreactive thereby inhibiting multilayer formation. Epitaxially grown SiGe with varying concentrations of Ge were used in this study. As-received, the amount of Ge in the SiGe wafers provided was

stated to be 18, 30 and 60 %. Representative XTEM images are show in **Figure 2**. Though chemical reactions on Si and Ge are similar there are variations in reactivity between the two materials. For example, the reaction of an alkene with hydrogen terminated Si will occur in solution when heated to 180 ^{o}C but under these same conditions it will not react with Ge. Either much higher temperatures (> 220 ^{o}C) or UV light are required for the reaction between an alkene and Ge to proceed. [35, 36]

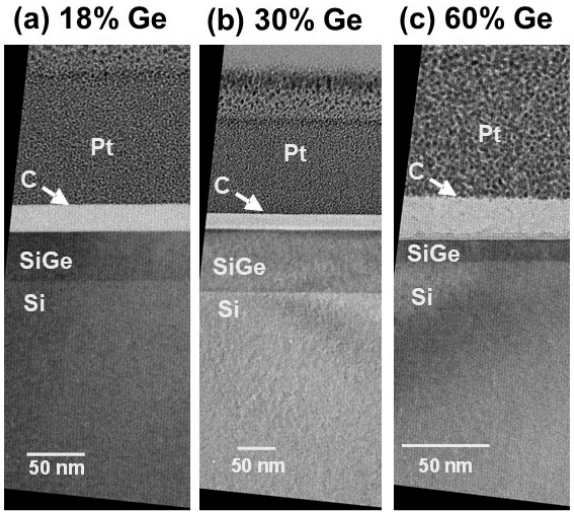

Figure 2: XTEM of as-received SiGe (a) 18% Ge (b) 30% Ge and (c) 60% Ge

Though the bulk SiGe wafers provided are stated to have 18, 30 and 60 % Ge in the epitaxial SiGe layers it does not necessarily mean that the surface stoichiometry is the same as the bulk. The surface stoichiometry is important as it may impact the chosen reaction conditions for the chemical functionalization. In order to assess if surface stoichiometries differ to the bulk, an angle-resolved XPS study was carried out. **Table 1** show the measured stoichiometries for each sample.

Table 1: The experimentally measured surface stoichiometries of the epitaxial SiGe. The measured stoichiometries are reported for take-off angles of 90 and 60 degrees, The measured stoichiometries are calculated from the areas of the Si *2p* and Ge *3d* XPS core levels, normalized using the appropriate relative sensitivity factors.

Sample ID	Measured stoichiometry	Measured stoichiometry (60°)
SiGe18	$Si_{0.86}Ge_{0.14}$	$Si_{0.88}Ge_{0.12}$
SiGe30	$Si_{0.67}Ge_{0.33}$	$Si_{0.69}Ge_{0.31}$
SiGe60	$Si_{0.35}Ge_{0.65}$	$Si_{0.35}Ge_{0.65}$

The measured stoichiometries are 14, 33 and 65 % for XPS with a take-off angle of 90° which corresponds to a sampling depth of 9.1 nm for the Ge 3d peak and 8.8 nm for Si 2p peak.[39] Those measured for the XPS with a take-off angle of 60° were 12, 31 and 65 %, where the sampling depth is halved when compared with samples measured with a take-off angle of 90° and thus are more surface sensitive. With a commonly specified error range of +/- 10 % it can be concluded that the surface and bulk stoichiometries do not differ drastically.

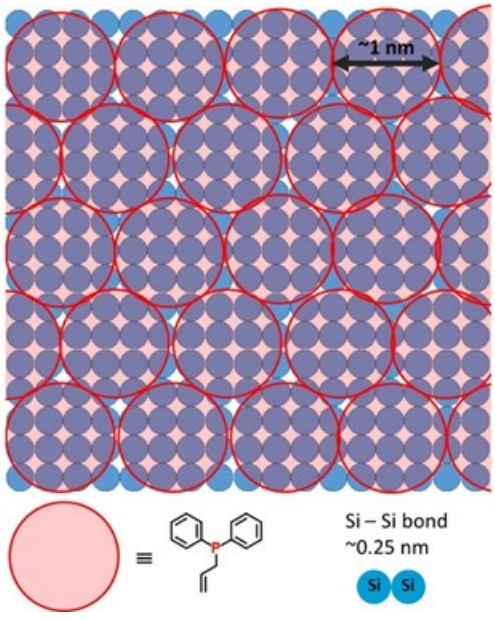

Figure 3: Illustration showing the approximate footprint of the molecule, ADP, on the surface of silicon.

Figure 3 shows roughly how much space the ADP will take up on the surface of a substrate. For the purposes of illustration the surface depicted is silicon. Given that ADP has an approximate molecular footprint of 1 nm^2 and that the Si-Si bond length in crystalline Si is roughly 0.25 nm about 1 in 16 Si atoms (or ~6 % of the surface atoms) will have a molecule bonded to them. An assumption is made here that these calculations will be very similar for the SiGe substrates. Though these calculations and the illustration in **Figure 3** are for indication only, when combined with the XPS data we are satisfied that we can treat the SiGe surface, from a chemical reactivity point of view, as if it were silicon. It should be noted that the authors recognize that though the chemical reactivity of Si and Ge are well established [28, 29, 36, 37]there is no available data on the reactivity of SiGe.

The selection of the drive-in anneal temperature is a critical part of this experimental set-up. Si melts at 1416 °C, while Ge melts at 938 °C, and alloys of SiGe melt at temperatures between those extremes, depending on the % Ge content. Another consideration is that the epitaxial SiGe is strained and heating to high temperatures will cause strain relaxation. XTEM and AFM were carried out on SiGe 30 % to assess the impact of annealing at high temperature. The standard annealing temperature for MLD on Si is 1050 °C. [26, 32] Before anneal, the substrates show no obvious crystal defects in cross-section or in the AFM analysis (representative images in **Figure 4a**). Post-anneal at 1050 °C, it is obvious the SiGe layer has been degraded (**Figures 4b**). For example, there is extensive crosshatching in the AFM. Crosshatching occurs as a result of misfit dislocations having formed at the SiGe:Si interface. These misfit dislocations are an indication of the strain relaxation which can also be seen in the XTEM which contains a noticeably defective SiGe:Si interface. Furthermore a stacking fault is visible in **Figure 4b** resulting in a kink or step-like feature at the surface where it terminates.

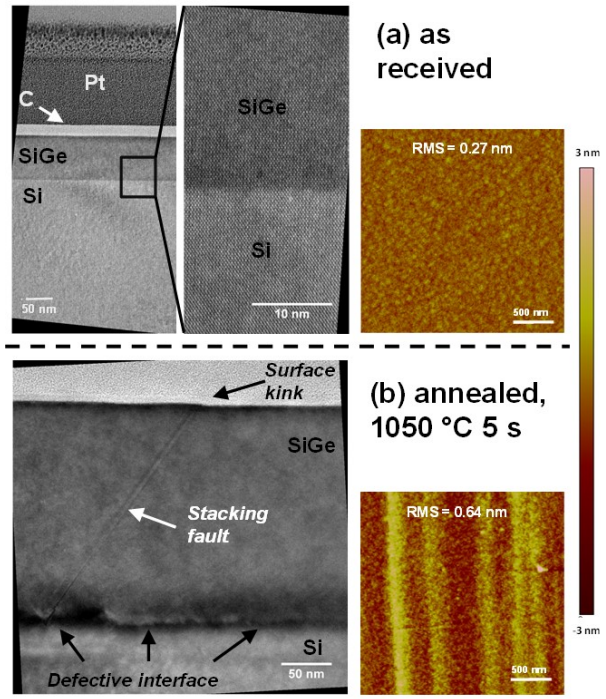

Figure 4: XTEM and AFM of as received SiGe 30 % (top row) and SiGe 30 % after annealing at 1050 °C for 5 seconds (bottom row).

Due to this degradation it is assumed that a 1050 °C RTA used for Si cannot be applied to Ge, and thus we are unable to apply a constant RTA temperature across all the SiGe alloys studied here. Instead we have chosen an RTA temperature at a fixed amount below the melting temperature of each material, in accordance with **Figure 5**. As 1050 °C is routinely used for P in-diffusion into Si,[34] we used this as our basis for a constant T_{melt} - T_{RTA} (1416-1050 °C) value. The RTA temperatures for 18, 30, and 60 % Ge content SiGe are thus 935, 835 and 685 °C respectively.

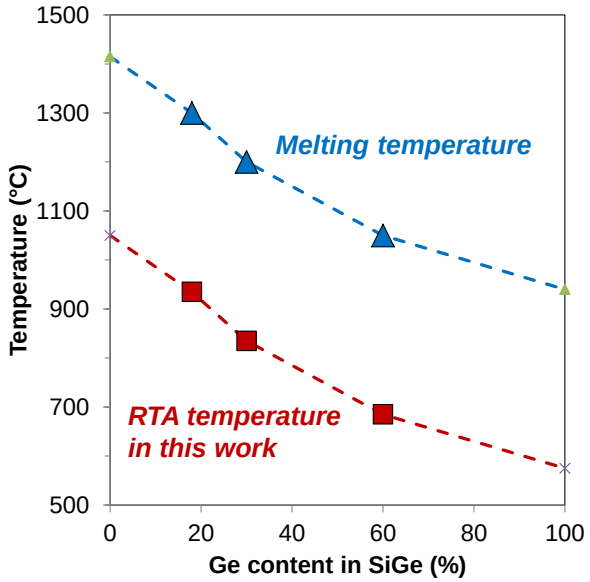

Figure 5: Melting temperature of SiGe as a function of Ge content. The dopant drive-in RTA was chosen to be a constant value below the melting temperature, also plotted here.

Figure 6 shows AFM images of all SiGe samples before and after MLD processing. Samples before MLD show that the surface topology is very uniform, with RMS values <0.3 nm. MLD processing leads to a small increase in all RMS values which is to be expected with wet chemistry processing and cap addition/removal possibly leaving residue on the sample surface. Disregarding these residues due to processing which are clearly present on the 18 and 60 % after MLD, all surfaces are of good quality. Though not quantified it is clear that crosshatching can be seen in both the 30 and 60 % samples which is an indicator of the onset of strain relaxation. [40, 41]

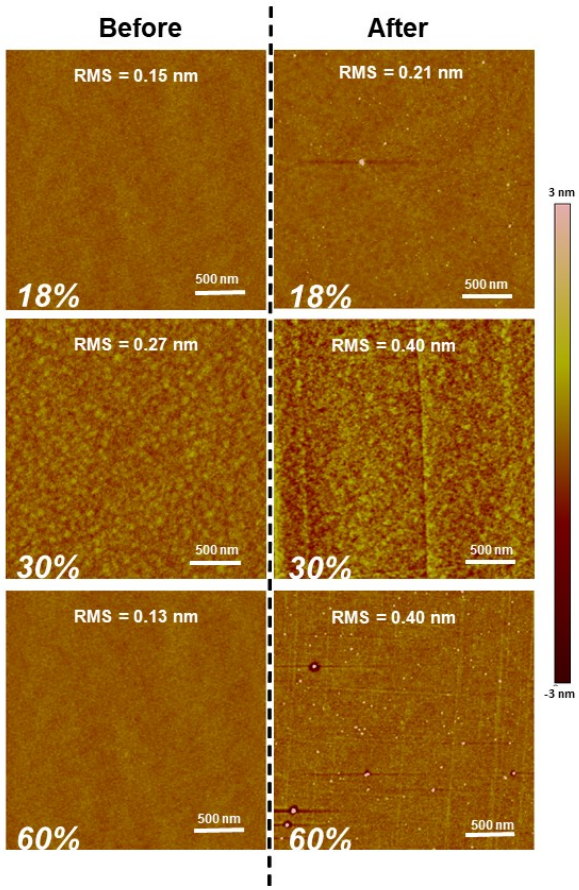

Figure 6: AFM before (left column) and after MLD (right column) of (a) 18 % SiGe (b) 30 % SiGe and (c) 60 % SiGe.

The impact of MLD on SiGe sample quality was further probed using X-TEM. **Figure 7** shows images of SiGe 30 % before and after MLD. It is clear from these images that P-diffusion into the SiGe30 sample does not lead to any crystalline damage at the temperature used in this study. This agrees with numerous other studies which demonstrate MLD as a non-destructive doping technique. [26,42] The SiGe:Si interface in **Figure 7** does not show any evidence of defects which leads us to believe that the small amount of crosshatching seen in AFM after MLD is inconsequential.

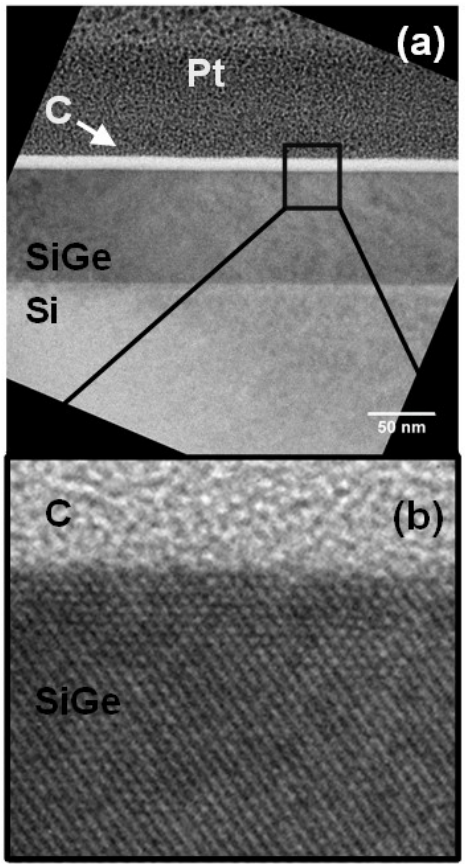

Figure 7: (a) XTEM of SiGe30 after MLD (b) Magnified region showing smooth interface and crystalline SiGe.

If defect formation as a results of strain relaxation of the SiGe layer was not considered problematic it would be possible to utilize higher anneal temperatures up to those seen in **Figure 4** (1050 °C). These higher anneal temperatures would theoretically enable higher in-diffusion and activation of the P dopant atoms. Previous studies on silicon have found that optimal RTA temperatures for P in-diffusion and activation were somewhere in the region of 1000-1100 °C.[26, 32] Another approach which may have the potential to reduce the probability of nucleating defects at the Si/SiGe interface seen at higher anneal temperatures (**Figure 4**) is the use of buffer layers. These buffer layers include a gradual increase in germanium content which leads to a smaller lattice mismatch than what is seen in samples where high Ge content SiGe has been grown directly on Si. Alternative annealing methods such as laser annealing have also been shown to work effectively in combination with ion implantation to dope strained

SiGe layers. [43] Combining laser annealing and MLD may prove to be a more suitable means than RTA, of achieving highly doped SiGe layers while maintaining the strained nature of the SiGe layer.

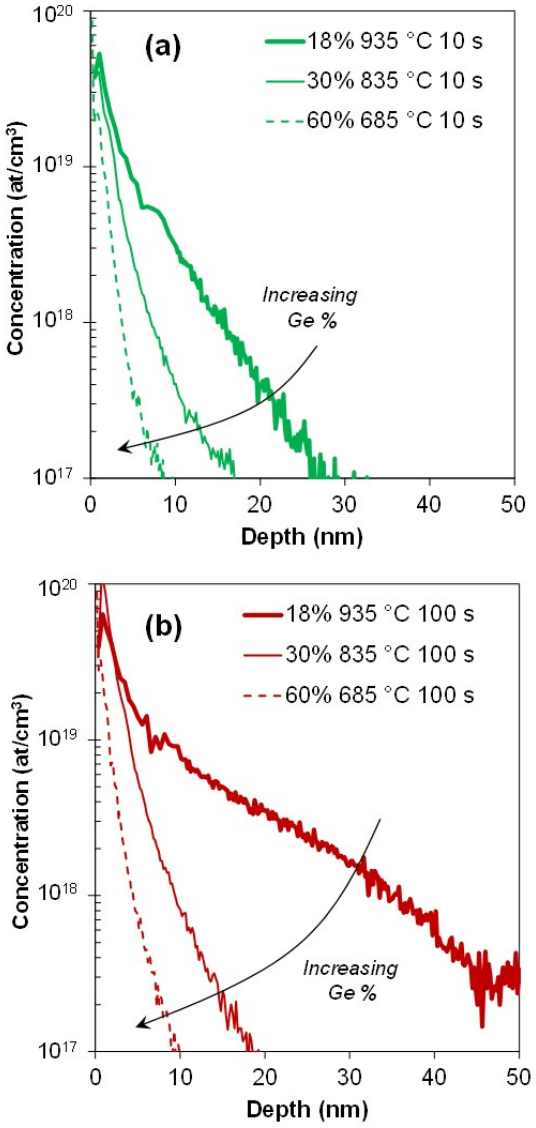

Figure 8: SIMS of P MLD doped SiGe with concentration of 18%, 30 % and 60 % with respective annealing temperatures of 935, 835 and 685 °C at annealing times of (a) 10 s (b) 100 s.

Figure 8 shows SIMS analysis of the concentration of P versus depth for the SiGe samples doped using MLD. From both **Figure 8a** and **8b** we note that less P diffusion occurs as the Ge content increases, again within the experimental framework of a constant T_{melt} - T_{RTA},

as the profiles for 18 % Ge content SiGe are deeper than those in 30 % Ge content SiGe, which are again deeper than those in 60 % Ge content SiGe. The longer anneal time produced more diffusion, which is consistent with theory, as dopant diffusion lengths are proportional to $\sqrt{t}$, where t is anneal time.[44] Based on the TEM images of the as-received SiGe layers, the dopant profiles in **Figure 8** are all contained within the SiGe layers, for the most part, and have not diffused into the underlying Si substrate.

Figure 9 shows P-diffusivity (D) in SiGe as a function of Ge content, at the specific temperatures used for the drive-in anneal. The blue points are data extracted from our experiments, while the black points are the data we could find in literature for similar temperatures and material compositions.[45-49] . The two blue points represent values extracted from the two annealing times, namely 10 and 100 s, as shown in **Figure 8.**

Note that the literature value temperatures and Ge content correspond to the experimental data we have in this work. In the literature, phosphorus D is presented as a function of 1/kT, and so for the specific content (e.g. 18% Ge) we could read off the D value for the corresponding temperature in this work (e.g. 935 °C). Overall the values extracted from our data correspond with the trends previously reported in literature. D drops with increasing Ge content and decreasing RTA temperature when using a constant T_{melt} - T_{RTA}.

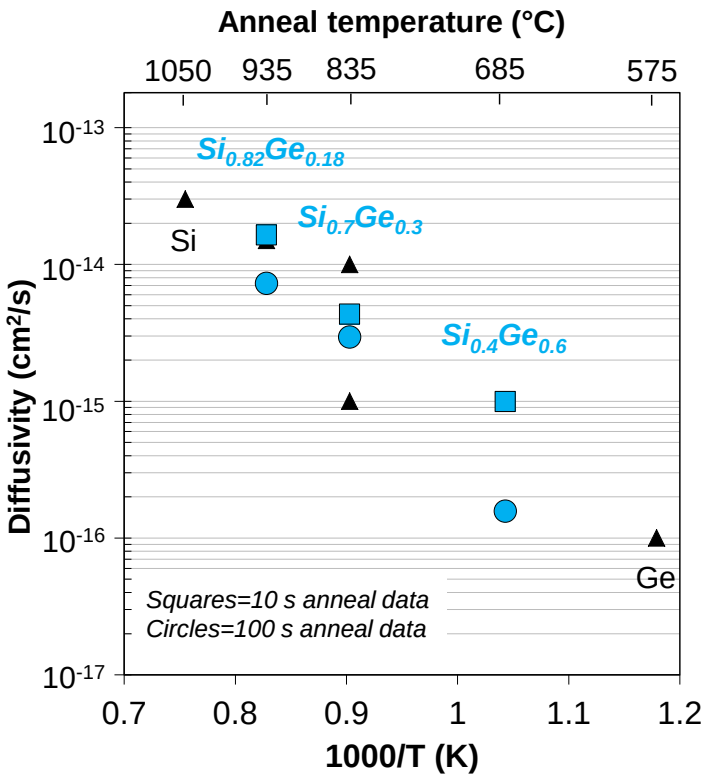

Figure 9: Phosphorus diffusivity in SiGe versus 1000/T extracted from our experiments (blue symbols) as well as literature values (black symbols). In this case T is the temperature of the drive-in anneal, which was kept at a constant value below the melting temperature of the material.

The method for extracting D for in-diffused doping profiles is now briefly summarized. The impurity concentration (C) profile for a chemical pre-deposition process has the form

$$C_{(x,t)} = C_s erfc\left(\frac{x}{2\sqrt{Dt}}\right) \qquad (1)$$

where x is the distance from the surface, t is time, C_s is the impurity surface concentration, and D is the impurity diffusivity. If D is constant, the depth of the profile depends only on time, and the surface concentration remains fixed as this is limited by solid solubility limit at that processing temperature. If the total quantity of dopant is defined as dose, Q, then this can be described as

$$Q_{(t)} = \int_0^\infty C_{(x,t)} dx \quad (2)$$

Using these two equations, the total incorporated dose can be simplified as

$$Q_{(t)} = \frac{2}{\sqrt{\pi}} C_s \sqrt{Dt} \quad (3)$$

Using the SIMS analysis in **Figure 5**, Q and C_s can be extracted. Knowing the experimental processing time, t, means D is the only unknown, and thus can be calculated. Factors that affect changes in dopant diffusivity in semiconductors include the relative dominance of interstitial-mediated or vacancy-mediated diffusion mechanisms, point defect populations, lattice strain, presence or absence of threading dislocations and their density, and finally the dose or supply of dopant. P diffusion in Si is predominantly interstitial-mediated,[50, 51] while P diffusion in Ge is vacancy-mediated.[45, 52] It is not clear presently at what point along the Ge % content axis where it changes from one mechanism to the other. From the evidence in **Figure 6** diffusivity changes quite linearly rather than reaching a toggle point or falling off a cliff, so probably the switch from interstitial or vacancy mediation is gradual.

Note that this is a simplified model for the purposes of our discussion, although it is well-known as a surface-source in-diffusion model. The system under study is very complicated considering the changing alloy composition will affect diffusion mechanisms, probability of dopant-point defect pairing, intrinsic concentrations of those point defects, both charged and uncharged, as well the presence of strain and extended defects. It is not the aim of this work to go into depth of the changing diffusion mechanisms as it would be another, quite-substantial, work. Furthermore, we have not explicitly considered a dependence of D on phosphorus concentration in this surface-source in-diffusion model, mainly as concentration enhancement effects usually arise at concentrations approaching or above 10^{20} at./cm^3 and we

are below those concentrations in this work. Nevertheless it is important to note that we have benchmarked our results with existing reports, and the data appear consistent.

The influence of strain should also be mentioned as these SiGe layers are grown directly on a Si substrate, without a strain-relaxed-buffer (SRB). Pakfar *et. al* modelled the effects of strain and Ge content on point defect population in SiGe,[53] which drive a change in dopant diffusivity. For P it was found that the effect of stress counterbalances the Ge chemical effect on interstitials, and thus the change in diffusivity is minimized. Note, we should state again that it was not the aim of this work to explore strain as one of the variables here, but rather to explore the choice of RTA temperature in the trade-off between successful dopant incorporation while avoiding epitaxial layer structural relaxation. Given the 2 orders of magnitude change in D as a function of RTA temperature, that is a dominant variable here.

As seen in the TEM and AFM data, with high thermal budgets threading dislocations will form in order to relax the strained layer. The threading dislocation density (TDD) will affect the diffusivity if the material is extremely defective as these defects could form preferential pathways for P atoms to diffuse.[54] However the data presented in **Figure 6** and **7** show that the TDD is less for the RTA temperatures considered in **Figure 8** and **9** then for the standard anneal temperature of 1050 ^{o}C. Although overall the TDD should not have a strong bearing on the conclusions in this work we cannot conclusively state that the trend in SIMS profiles in Figure 8 are not contributed to by the TDD.

Finally, Si and Ge inter-diffusion has been modelled by Zechner and Zographos,[55] which may locally affect the SiGe composition close to the SiGe-Si interface. The change in Ge % content will have a knock-on effect on point-defect populations and hence point-defect mediated dopant diffusion, as discussed earlier. For the study here, namely in-diffusion from the top surface, the back interface of the SiGe (away from the source of the dopant) should only have a minimal effect on the dopant drive-in.

CONCLUSIONS

This paper has outlined the application of MLD to SiGe showing both the advantages of this form of doping and some of the issues which must be overcome for future use. Ultra-shallow doping has been achieved with phosphorus dopant atoms to levels currently in the region of 2×10^{19} atoms/cm^{-3}. Doping levels in excess of 1×10^{20} atoms/cm^{-3} are required for working devices and the authors are working on combining MLD with advanced annealing processes (e.g. laser annealing) to achieve these values. Diffusivity levels found during this study agree with values from literature for P diffusion in strained SiGe. Strain relaxation is a major issue when applying high thermal budget treatments to epitaxially grown SiGe/Si substrates. In this study we have optimized RTA temperatures for low to high Ge content SiGe samples to produce maximum doping levels without introducing strain relaxation into the substrates. More advanced annealing methods or the use of buffer layers would allow for greater dopant incorporation while maintaining the strained nature of the SiGe layer.

ACKNOWLEDGEMENTS

This work is supported by Enterprise Ireland through the projects IP-2015-0368 and IP-2017-0605, and by the European Union through the European Regional Development Fund (ERDF) under Ireland's European Structural and Investment Funds Programmes 2014-2020.

REFERENCES

1. O. Engström, B. Raeissi, S. Hall, O. Buiu, M. C. Lemme, H. D. B. Gottlob, P. K. Hurley and K. Cherkaoui, Solid-State Electronics **51** (4 SPEC. ISS.), 622-626 (2007).
2. M. J. H. Van Dal, N. Collaert, G. Doornbos, G. Vellianitis, G. Curatola, B. J. Pawlak, R. Duffy, C. Jonville, B. Degroote, E. Altamirano, E. Kunnen, M. Demand, S. Beckx, T. Vandeweyer, C. Delvaux, F. Leys, A. Hikavyy, R. Rooyackers, M. Kaiser, R. G. R. Weemaes, S. Biesemans, M. Jurczak, K. Anil, L. Witters and R. J. P. Lander, Digest of Technical Papers - Symposium on VLSI Technology, 110-111 (2007).
3. J. Franco, B. Kaczer, J. Mitard, M. Toledano-Luque, G. Eneman, P. J. Roussel, M. Cho, T. Kauerauf, L. Witters, A. Hikavyy, G. Hellings, L. Å. Ragnarsson, N. Horiguchi, T. Grasser, M. Heyns and G. Groeseneken, ECS Transactions **50**, 177-195 (2012).
4. A. Shickova, P. Verheyen, G. Eneman, R. Degraeve, E. Simoen, P. Favia, D. O. Klenov, E. San Andres, B. Kaczer, M. Jurczak, P. Absil, H. E. Maes and G. Groeseneken, IEEE Transactions on Electron Devices **55** (12), 3432-3441 (2008).
5. G. Eneman, S. Yamaguchi, C. Ortolland, S. Takeoka, L. Witters, T. Chiarella, P. Favia, A. Hikavyy, J. Mitard, M. Kobayashi, R. Krom, H. Bender, J. Tseng, W. E. Wang, W. Vandervorst, R. Loo, P. P. Absil, S. Biesemans and T. Hoffmann, Digest of Technical Papers - Symposium on VLSI Technology, 41-42 (2010).
6. M. Togo, J. W. Lee, L. Pantisano, T. Chiarella, R. Ritzenthaler, R. Krom, A. Hikavyy, R. Loo, E. Rosseel, S. Brus, J. W. Maes, V. MacHkaoutsan, J. Tolle, G. Eneman, A. D. Keersgieter, G. Boccardi, G. Mannaert, S. E. Altamirano, S. Locorotondo, M. Demand, N. Horiguchi and A. Thean, Technical Digest - International Electron Devices Meeting, IEDM, 18.12.11-18.12.14 (2012).
7. P. Hashemi, T. Ando, K. Balakrishnan, S. Koswatta, K. L. Lee, J. A. Ott, K. Chan, J. Bruley, S. U. Engelmann, V. Narayanan, E. Leobandung and R. T. Mo, 2017 International Symposium on VLSI Technology, Systems and Application, VLSI-TSA 2017 (2017).
8. R. Xie, P. Montanini, K. Akarvardar, N. Tripathi, B. Haran, S. Johnson, T. Hook, B. Hamieh, D. Corliss, J. Wang, X. Miao, J. Sporre, J. Fronheiser, N. Loubet, M. Sung, S. Sieg, S. Mochizuki, C. Prindle, S. Seo, A. Greene, J. Shearer, A. Labonte, S. Fan, L. Liebmann, R. Chao, A. Arceo, K. Chung, K. Cheon, P. Adusumilli, H. P. Amanapu, Z. Bi, J. Cha, H. C. Chen, R. Conti, R. Galatage, O. Gluschenkov, V. Kamineni, K. Kim, C. Lee, F. Lie, Z. Liu, S. Mehta, E. Miller, H. Niimi, C. Niu, C. Park, D. Park, M. Raymond, B. Sahu, M. Sankarapandian, S. Siddiqui, R. Southwick, L. Sun, C. Surisetty, S. Tsai, S. Whang, P. Xu, Y. Xu, C. Yeh, P. Zeitzoff, J. Zhang, J. Li, J. Demarest, J. Arnold, D. Canaperi, D. Dunn, N. Felix, D. Gupta, H. Jagannathan, S. Kanakasabapathy, W. Kleemeier, C. Labelle, M. Mottura, P. Oldiges, S. Skordas, T. Standaert, T. Yamashita, M. Colburn, M. Na, V. Paruchuri, S. Lian, R. Divakaruni, T. Gow, S. Lee, A. Knorr, H. Bu and M. Khare, Technical Digest - International Electron Devices Meeting, IEDM, 2.7.1-2.7.4 (2017).
9. A. Ahmed, R. B. Dunford, D. J. Paul, M. Pepper, A. C. Churchill, D. J. Robbins and A. J. Pidduck, Thin Solid Films **369** (1), 324-327 (2000).
10. J. Zhang, S. G. Turner, S. Y. Chiam, R. Liu, E. S. Tok, A. T. S. Wee, A. C. H. Huan, I. Kelly and C. P. A. Mulcahy, Surface Science **600** (11), 2288-2292 (2006).
11. D. Li, X. Zhao, L. Wang, B. Conrad, A. Soeriyadi, A. Lochtefeld, A. Gerger, I. Perez-Wurfl and A. Barnett, Applied Physics Letters **109** (24) (2016).
12. L. Wang, D. Li, X. Zhao, B. Conrad, M. Diaz, A. Soeriyadi, A. Lochtefeld, A. Gerger, I. Perez-Wurfl and A. Barnett, Physica Status Solidi - Rapid Research Letters **10** (8), 596-599 (2016).
13. X. Zhao, D. Li, T. Zhang, B. Conrad, L. Wang, A. H. Soeriyadi, J. Han, M. Diaz, A. Lochtefeld, A. Gerger, I. Perez-Wurfl and A. Barnett, Solar Energy Materials and Solar Cells **159**, 86-93 (2017).
14. A. Renau, ECS Transactions **35**, 173-184 (2011).
15. M. I. Current, in *Industrial Accelerators and their Applications* (2012), pp. 9-56.
16. R. Duffy, M. J. H. Van Dal, B. J. Pawlak, M. Kaiser, R. G. R. Weemaes, B. Degroote, E. Kunnen and E. Altamirano, Applied Physics Letters **90** (24) (2007).

17. J. Mody, R. Duffy, P. Eyben, J. Goossens, A. Moussa, W. Polspoel, B. Berghmans, M. J. H. Van Dal, B. J. Pawlak, M. Kaiser, R. G. R. Weemaes and W. Vandervorst, Journal of Vacuum Science and Technology B: Microelectronics and Nanometer Structures **28** (1), C1H5-C1H13 (2010).
18. Y. Sasaki, K. Okashita, B. Mizuo, M. Kubota, M. Ogura and O. Nishijima, Journal of Applied Physics **111** (1) (2012).
19. S. Sen, J. Siejka, A. Savtchouk and J. Lagowski, Applied Physics Letters **70** (17), 2253-2255 (1997).
20. Y. Liu, K. Koga, S. Khumpuang, M. Nagao, T. Matsukawa and S. Hara, Japanese Journal of Applied Physics **56** (6) (2017).
21. S. Shintri, C. Yong, B. Zhu, S. Byrappa, B. Fu, H. C. Lo, D. Choi and V. Kolagunta, Materials Science in Semiconductor Processing **82**, 9-13 (2018).
22. J. H. Comfort, E. F. Crabbe, J. D. Cressler, W. Lee, J. Y. C. Sun, J. Malinowski, M. D'Agostino, J. N. Burghartz, J. M. C. Stork and B. S. Meyerson, Technical Digest - International Electron Devices Meeting, IEDM **1991-January**, 857-860 (1991).
23. S. Gannavaram, N. Pesovic and M. C. Öztürk, Technical Digest - International Electron Devices Meeting, 437-440 (2000).
24. S. G. Kim, G. S. Kim, S. H. Kim and H. Y. Yu, IEEE Electron Device Letters **39** (12), 1828-1831 (2018).
25. J. Veerbeek, L. Ye, W. Vijselaar, T. Kudernac, W. G. van der Wiel and J. Huskens, Nanoscale **9** (8), 2836-2844 (2017).
26. R. Duffy, A. Ricchio, R. Murphy, G. Maxwell, R. Murphy, G. Piaszenski, N. Petkov, A. Hydes, D. O'Connell, C. Lyons, N. Kennedy, B. Sheehan, M. Schmidt, F. Crupi, J. D. Holmes, P. K. Hurley, J. Connolly, C. Hatem and B. Long, Journal of Applied Physics **123** (12) (2018).
27. O. Hazut, A. Agarwala, T. Subramani, S. Waichman and R. Yerushalmi, Jove-Journal of Visualized Experiments (82), 5 (2013).
28. J. C. Ho, R. Yerushalmi, Z. A. Jacobson, Z. Fan, R. L. Alley and A. Javey, Nature Materials **7** (1), 62-67 (2008).
29. P. Taheri, H. M. Fahad, M. Tosun, M. Hettick, D. Kiriya, K. Chen and A. Javey, Acs Applied Materials & Interfaces **9** (24), 20648-20655 (2017).
30. J. C. Ho, R. Yerushalmi, G. Smith, P. Majhi, J. Bennett, J. Halim, V. N. Faifer and A. Javey, Nano Letters **9** (2), 725-730 (2009).
31. T. Alphazan, L. Mathey, M. Schwarzwalder, T. H. Lin, A. J. Rossini, R. Wischert, V. Enyedi, H. Fontaine, M. Veillerot, A. Lesage, L. Emsley, L. Veyre, F. Martin, C. Thieuleux and C. Coperet, Chemistry of Materials **28** (11), 3634-3640 (2016).
32. N. Kennedy, R. Duffy, L. Eaton, D. O'Connell, S. Monaghan, S. Garvey, J. Connolly, C. Hatem, J. D. Holmes and B. Long, Beilstein Journal of Nanotechnology **9** (1), 2106-2113 (2018).
33. J. O'Connell, G. Collins, G. P. McGlacken, R. Duffy and J. D. Holmes, Acs Applied Materials & Interfaces **8** (6), 4101-4108 (2016).
34. M. van Druenen, G. Collins, C. Glynn, C. O'Dwyer and J. D. Holmes, Acs Applied Materials & Interfaces **10** (2), 2191-2201 (2018).
35. B. Long, G. A. Verni, J. O'Connell, J. Holmes, M. Shayesteh, D. O'Connell, R. Duffy and Ieee, 2014 20th International Conference on Ion Implantation Technology (Iit 2014), 4 (2014).
36. B. Long, G. A. Verni, J. O'Connell, M. Shayesteh, A. Gangnaik, Y. M. Georgiev, P. Carolan, D. O'Connell, K. J. Kuhn, S. B. Clendenning, R. Nagle, R. Duffy and J. D. Holmes, Materials Science in Semiconductor Processing **62**, 196-200 (2017).
37. F. Sgarbossa, S. M. Carturan, D. De Salvador, G. A. Rizzi, E. Napolitani, G. Maggioni, W. Raniero, D. R. Napoli, G. Granozzi and A. Carnera, Nanotechnology **29** (46), 11 (2018).
38. J. O'Connell, E. Napolitani, G. Impellizzeri, C. Glynn, G. P. McGlacken, C. O'Dwyer, R. Duffy and J. D. Holmes, Acs Omega **2** (5), 1750-1759 (2017).
39. S. Tanuma, C. J. Powell and D. R. Penn, Surface and Interface Analysis **43** (3), 689-713 (2011).

40. H. Chen, Y. K. Li, C. S. Peng, H. F. Liu, Y. L. Liu, Q. Huang, J. M. Zhou and Q. K. Xue, Physical Review B **65** (23), 4 (2002).
41. T. Egawa, A. Sakai, T. Yamamoto, N. Taoka, O. Nakatsuka, S. Zaima and Y. Yasuda, Applied Surface Science **224** (1-4), 104-107 (2004).
42. O. C. John, B. Subhajit, D. Ray and H. J. D, edited by S. Biswas (Nanotechnology, Nanotechnology, 2016).
43. G. V. Luong, S. Wirths, S. Stefanov, B. Hollander, J. Schubert, J. C. Conde, T. Stoica, U. Breuer, S. Chiussi, M. Goryll, D. Buca and S. Mantl, Journal of Applied Physics **113** (20), 9 (2013).
44. P. M. Fahey, P. B. Griffin and J. D. Plummer, Reviews of Modern Physics **61** (2), 289-384 (1989).
45. S. Brotzmann and H. Bracht, Journal of Applied Physics **103** (3) (2008).
46. J. S. Christensen, H. H. Radamson, A. Y. Kuznetsov and B. G. Svensson, Journal of Applied Physics **94** (10), 6533-6540 (2003).
47. N. R. Zangenberg, J. Fage-Pedersen, J. L. Hansen and A. N. Larsen, Journal of Applied Physics **94** (6), 3883-3890 (2003).
48. D. Mathiot and J. C. Dupuy, Applied Physics Letters **59** (1), 93-95 (1991).
49. P. Pichler, *Intrinsic Point Defects, Impurities, and Their Diffusion in Silicon*. (Springer, Wien, Austria, 2004).
50. J. Xu, V. Krishnamoorthy, K. S. Jones and M. E. Law, Journal of Applied Physics **81** (1), 107-111 (1997).
51. N. E. B. Cowern, D. J. Godfrey and D. E. Sykes, Applied Physics Letters **49** (25), 1711-1713 (1986).
52. M. Naganawa, Y. Shimizu, M. Uematsu, K. M. Itoh, K. Sawano, Y. Shiraki and E. E. Haller, Applied Physics Letters **93** (19) (2008).
53. A. Pakfar, Materials Science and Engineering B: Solid-State Materials for Advanced Technology **89** (1-3), 225-228 (2002).
54. N. Kuroda, C. Sasaoka, A. Kimura, A. Usui and Y. Mochizuki, Journal of Crystal Growth **189-190**, 551-555 (1998).
55. C. Zechner and N. Zographos, Materials Science in Semiconductor Processing **42**, 230-234 (2016).